



Roller bearing acoustic signature extraction by wavelet packet transform, applications in fault detection and size estimation



Farzad Hemmati ^{a,*}, Wasim Orfali ^b, Mohamed S. Gadala ^a

^a Mechanical Engineering Dept., University of British Columbia, 2054-6250 Applied Science Lane, Vancouver, BC V6T 1Z4, Canada

^b Faculty of Engineering, Taibah University, Al Madina Al Munawara, Saudi Arabia

ARTICLE INFO

Article history:

Received 15 December 2014

Received in revised form 3 July 2015

Accepted 10 November 2015

Available online 28 November 2015

Keywords:

Rolling element bearing

Acoustic emission signals

Condition monitoring

Wavelet packet transform

Statistical analysis

Defect size calculation

ABSTRACT

Continuous online monitoring of rotating machines is necessary to assess real-time health conditions so as to enable early detection of operation problems and thus reduce the possibility of downtime. Rolling element bearings are crucial parts of many machines and there has been an increasing demand to find effective and reliable health monitoring technique and advanced signal processing to detect and diagnose the size and location of incipient defects. Condition monitoring of rolling element bearings, comprises four main stages which are, statistical analysis, fault diagnostics, defect size calculation, and prognostics. In this paper the effect of defect size, operating speed, and loading conditions on statistical parameters of acoustic emission (AE) signals, using design of experiment method (DOE), have been investigated to select the most sensitive parameters for diagnosing incipient faults and defect growth on rolling element bearings. A modified and effective signal processing algorithm is designed to diagnose localized defects on rolling element bearings components under different operating speeds, loadings, and defect sizes. The algorithm is based on optimizing the ratio of Kurtosis and Shannon entropy to obtain the optimal band pass filter utilizing wavelet packet transform (WPT) and envelope detection. Results show the superiority of the developed algorithm and its effectiveness in extracting bearing characteristic frequencies from the raw acoustic emission signals masked by background noise under different operating conditions. To experimentally measure the defect size on rolling element bearings using acoustic emission technique, the proposed method along with spectrum of squared Hilbert transform are performed under different rotating speeds, loading conditions, and defect sizes to measure the time difference between the double AE impulses. Measurement results show the power of the proposed method for experimentally measuring size of different fault shapes using acoustic emission signals.

© 2015 Elsevier Ltd. All rights reserved.

1. Introduction

Condition monitoring of heavy rotating machinery and equipment such as turbines, compressors and generators, is gaining importance in various industries since it keeps the plant at healthy condition for maximum production; helps in detecting faults at early stages; avoid serious accidents and damage; and reduces downtime. Bearings are the common elements used in heavy rotating machinery and equipment because of their high reliability. Bearings start to malfunction due to machine overload, shaft misalignment, rotor unbalance, overheating, etc. Many different techniques based on vibration methods have been developed to extract bearing fault features [1]. However, vibration signals are

not sensitive to incipient faults and they are usually masked by background noise caused by mechanical vibration signals from rotating machinery. Hence, it is normally difficult for the vibration techniques to detect bearing faults at an early stage. Acoustic emission (AE) is the phenomenon of transient elastic wave generation due to a rapid release of strain energy caused by relative motion of small particles under mechanical stresses [2]. Interaction of rolling element bearing components and movement of bearing rollers over defects will produce AE's. The frequency content of acoustic emission (AE) is typically in the range of 100 kHz to 1 MHz, so AE is not influenced or distorted by imbalance and misalignment which are at low frequency ranges. The high sensitivity of AE technique and AE parameters in detecting the incipient bearing faults has become one of the significant advantages of AE over vibration measurement [3]. A comprehensive review of AE application for bearing fault detection was presented by Mba and Rao [4]. Al-Ghamdi and Mba [5] investigated the relationship between AE

* Corresponding author. Tel.: +1 (604) 649 4574.

E-mail addresses: fahemmatti@gmail.com (F. Hemmati), orfaliwasim@hotmail.com (W. Orfali), gadala@mech.ubc.ca (M.S. Gadala).

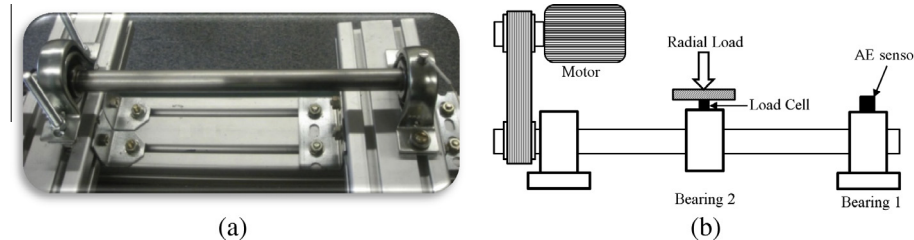


Fig. 1. (a) Experimental test setup, (b) experimental setup sketch.

Table 1
Bearing parameters.

Bearing specification	Timken 09074
Ball diameter (B_D)	7.2 (mm)
Pitch diameter (P_D)	33.5 (mm)
Number of rollers (n)	12
Contact angle (β)	8.3°
Bearing dynamic load capacity (C_{90})	10300 (N)

parameters in time domain and defect size. They concluded that AE burst duration is an effective parameter for identifying defect size on the outer race. However, in recent work performed by researchers there is no sensitivity analysis presented to analyze the most sensitive statistical parameter to incipient faults and defect growth. Acoustic based diagnostic signals in real industrial environments associated with high temperatures, rotating speeds, and pressures are always masked by high levels of noise. Desirable de-noising of these signals is not achievable with conventional techniques. Therefore, to overcome this challenge adaptive signal processing techniques need to be developed to enhance signal to noise ratio of AE signals. Dyer and Stewart [6] first presented the use of kurtosis parameter for bearing fault diagnosis and it was suggested to use kurtosis value in selected frequency bands. Antoni and Randall [7] presented the use of Spectral Kurtosis (SK) to extract transient components from a noisy signal. Sawalhi and Randall [8] proposed minimum entropy deconvolution (MED) technique along with SK to enhance the results of envelope analysis from a vibration bearing fault signal. Discrete wavelet transform (DWT) has been used in signal denoising due to its high resolution in time and frequency domains [9]. For instance, Qiu et al. [10] utilized wavelet filter-based denoising method to enhance weak periodic impulse signature masked by standard Gaussian white noise. In DWT, a digitized signal is decomposed into its low-pass approximation and high-pass detailed signals and further decompositions only apply to the detailed components. Hence, it suffers from insufficient treatment of the high frequency components where the bearing fault impulses exist [11]. Thus, wavelet packet transform (WPT) has been introduced to overcome this issue by treating both low and high frequency components [11]. Lei et al. [12] proposed an improved kurtogram method for diagnosing bearing faults. Even though, this method finds the frequency band which has the maximum value of kurtosis using WPT, the optimal wavelet function is not selected along with kurtosis value does not provide any information regarding periodic behavior of bearing fault impulses. In this paper, an experimental study

Table 3
Parameters range for sensitivity analyses of case study II.

	(−)	(+)
Defect size (D)	1 (mm)	2 (mm)
Rotating speed (R)	300 (rpm)	1100 (rpm)
Radial load (L)	0 (N)	100 (N)

Table 4
Example of Plackett–Burman design objective function with three parameters.

	Defect size	Speed	Load	Statistical parameter (R)
Exp.1	+	+	+	$R_1 = 5$
Exp.2	+	+	−	$R_2 = 10$
Exp.3	+	−	+	$R_3 = 15$
Exp.4	+	−	−	$R_4 = 2$
Exp.5	−	+	+	$R_5 = 4$
Exp.6	−	+	−	$R_6 = 17$
Exp.7	−	−	+	$R_7 = 22$
Exp.8	−	−	−	$R_8 = 12$
Sum	A_1	A_2	A_3	

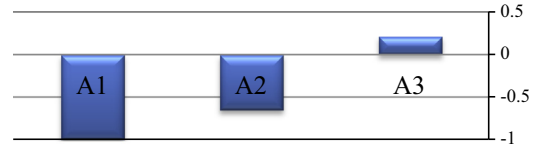


Fig. 2. Bar diagram of normalized objective function using Plackett–Burman design.

is presented to investigate the most sensitive statistical parameters for diagnosing defect growth and incipient faults in time domain analysis utilizing DOE method. A new approach based on selecting the optimal band-pass filter using WPT and selecting the optimal wavelet function is used in acoustic emission (AE) analysis to extract fault features, location of faults, and defect sizes. The outline of this paper is as follows: In Sections 2 and 3 the experimental setup and the experimental procedure for statistical analysis are explained. In Section 4 the background of DOE method is explained. In Section 5 the results of applying DOE method on the measured AE signals for sensitivity analysis are shown. In Section 6, the concept of wavelet packet transform (WPT), Shannon entropy, kurtogram, and Hilbert transform are reviewed. In Section 7, a new approach to select the optimal mother wavelet function is explained. In Section 8, the proposed method based on optimizing the kurtosis to Shannon entropy ratio of band-pass signal using WPT is discussed in detail and it is applied on a noisy impulse like signal. In this section, the proposed method is applied to the experimentally acquired signals of a faulty bearing where the faults are artificially introduced on a rolling element bearing to find the location and size of the defects. The results demonstrate that by selecting an optimal band-pass filter, bearing defects can be

Table 2
Parameters range for sensitivity analysis of case study I.

	(−)	(+)
Defect size (D)	0 (mm)	1 (mm)
Rotating speed (R)	300 (rpm)	1100 (rpm)
Radial load (L)	0 (N)	100 (N)

Table 5

Plackett–Burman design normalized objective function of the outer race line defect shape for case study I.

	Counts	PV	RMS	Kurtosis	Duration	CF	Skewness
Defect	1	1	1	1	1	1	-1
Speed	0.32	0.92	0.99	0.51	-0.58	0.24	-0.03
Load	-0.01	0.19	0.08	0.17	-0.06	0.17	0.16

detected and their sizes can be measured at an early stage of development.

2. Experimental setup

The experimental setup is consisted of a spindle, driven by a variable speed motor and a dismountable bearing test rig which is shown in Fig. 1(a) and (b). The spindle can be driven from 130 rpm up to 2200 rpm. A 09074 separable Timken tapered roller bearing is mounted on a pillow block in order to enhance the feasibility of introducing faults on the outer race and roller elements, moreover, assembly and disassembly of the bearing was accomplished with minimum disruption to the test setup. The distance between the defective bearing (Bearing 1) and motor is 50 cm. The Bearing parameters are tabulated in Table 1.

A second bearing was mounted in the middle of the shaft, which supports variable radial loads. The load was measured using load cell 247AS which has a capacity of 2000 N. The AE data acquisition and sensor used for the bearing fault diagnosis were NI and Physical Acoustic testing system respectively. The AE sensor (Nano-30 Physical Acoustic) was placed on the top of the bearing pillow block. The AE signals detected by the sensor were gained for 20 dB and all-pass filtered by the pre-amplifier (PAC 2/4/6c). The preprocessed signal is digitized by NI USB-6366 for data sampling at variable frequencies.

3. Statistical analysis experimental procedure

The most common signal processing technique is time domain statistical analysis. Signal analysis in time domain has been used to monitor simple machine conditions and faults utilizing statistical parameters. In this paper the most common acoustic emission and vibration statistical parameters, ring down counts (counts), peak value (PV), root mean square (RMS), kurtosis, burst duration (duration), crest factor (CF), and skewness [6,13,14], are used for statistical analysis of the measured acoustic emission (AE) signals of the rolling element bearing with a line defect shape on the outer race. Experimental tests were performed by first making the

defects in the appropriate size and geometrical shape. Bearing faults are artificially produced on the outer race using an engraving machine tool to control the shape and depth of the faults. All experiments have been conducted at rotating speeds of 300 rpm and 1100 rpm and under the loads of 0 N and 100 N (0.01 C₉₀). The sampling rate of data acquisition card is set to 2 MHz for all experiments and the recording time is 5 s. For each experiment, 10 waveforms are measured and the average value of statistical measurements are calculated and reported as the experimentally measured statistical values.

4. Design of experiment (DOE) method

Experimental design (also called Design of Experiments or DOE) is a collection of procedures and statistical tools for planning experiments and analyzing the results for examining how variations in parameters affect an objective function. Although experimental design techniques were originally developed for physical experiments, they also work very well with virtual experiments. DOE identifies which factors and combination of factors most affect the behavior of the system. First every factor is considered that may potentially affect the response and a DOE analysis is used to determine how much each contributes to the response. This helps in narrowing down further experimentations to just the important factors, and also ensures that significant factors will not be left out. DOE maybe followed by a more in depth experiment on the most important factors. This is accomplished by determining a set of experiments that are based on variations in a set of given parameters. It goes further than a simple sensitivity study because it considers not only the effect of small changes to each parameter independently, but also the interactions between parameters. PLACKETT–BURMAN design is one of DOE methods which provides the most accurate answer with the smallest number of experiments [15]. In this method first the most appropriate design matrix will be determined by the number of factors selected for the analysis. Once the experiment is run and the samples measured, the data from the experiment are used to calculate the effects and to determine the statistical significance of those effects. First the response (objective function) which are the statistical measurements, are calculated for each treatment combination, then working with the columns, the effect, which is the difference between the response at the high level and low level, is obtained (using the sign in the column). The results can also be normalized by dividing all values by their maximum, but we must take the sign into notice. A positive sign means that going from the low level to the high level cause an increase in the objective function, and vice versa.

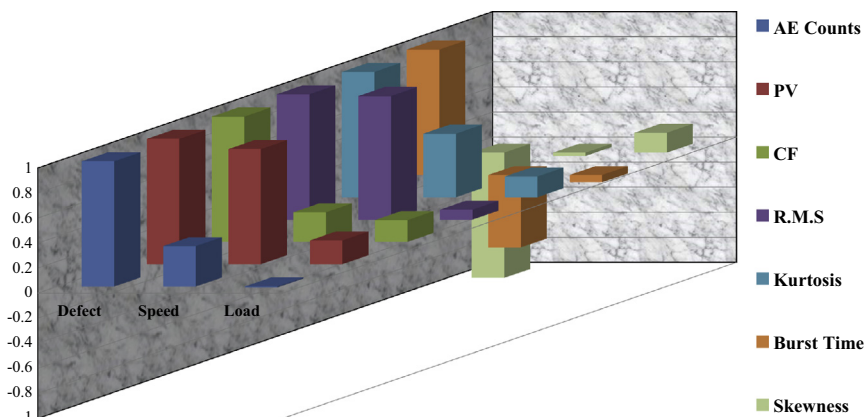


Fig. 3. Normalized effect of defect size, rotating speed, and radial load on the AE statistical parameters of the outer race line defect shape for case study I.

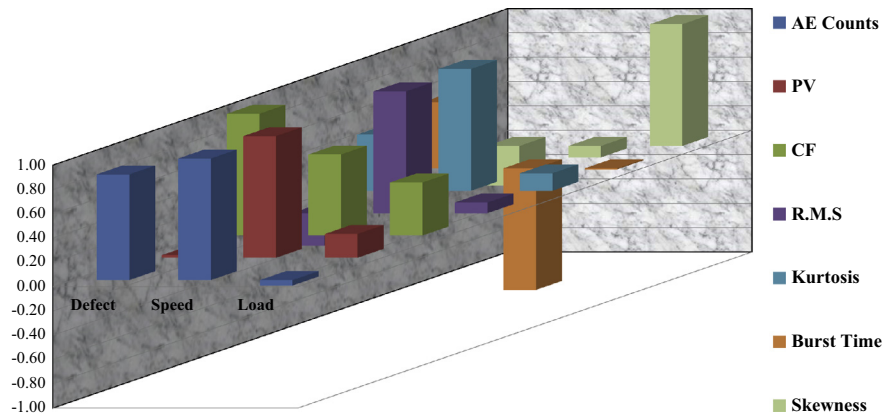


Fig. 4. Normalized effect of defect size, rotating speed, and radial load on the AE statistical parameters of the outer race line defect shape for case study II.

Table 6

Plackett-Burman design normalized objective function of the outer race line defect shape for case study II.

	Counts	PV	RMS	Kurtosis	Duration	CF	Skewness
Defect	0.87	0.02	-0.27	0.46	0.54	1	-0.32
Speed	1	1	1	1	-1	0.66	-0.09
Load	-0.04	0.20	0.09	0.14	-0.01	0.43	1

5. Sensitivity analysis of measured AE statistical parameters

In the experimental model, rolling element bearing setup shown in Fig. 1, defect size, rotating speed, and radial load have been considered as the most critical parameters that may influence the AE statistical values. Their minimum and maximum deviations for conducting the sensitivity analysis using DOE method for two case studies are tabulated in Tables 2 and 3. It should be noted that, linear changes in statistical parameters are observed for the following two case studies.

There are 8 designs and in each design the 3 above mentioned parameters are scaled according to their sign. In Tables 2 and 3, '+' shows the upper limit of the parameters and '-' shows the lower limit of the parameters. Then the objective function for each design is calculated based on the experimental result. The objective functions for this problem are the analyzed statistical parameters in this section (AE counts, peak value, RMS, kurtosis, burst duration, crest factor, and skewness). After calculating the objective functions for each design, the effect of each parameter is calculated and then normalized. A sample example of calculation of DOE method with three parameters is tabulated in Table 4 and its sensitivity is illustrated in Fig. 2. The last row of the Table 4 indicates the normalized effect, and Fig. 2 illustrates the effect in a bar diagram.

The values A_1 , A_2 , and A_3 are the summations of statistical parameters based on the signs in Table 4 and can be calculated as [15]:

$$\begin{aligned} A_1 &= R_1 + R_2 + R_3 + R_4 - R_5 - R_6 - R_7 - R_8 = -23/23 \\ A_2 &= R_1 + R_2 - R_3 - R_4 + R_5 + R_6 - R_7 - R_8 = -15/23 \\ A_3 &= R_1 - R_2 + R_3 - R_4 + R_5 - R_6 + R_7 - R_8 = 5/23 \end{aligned} \quad (1)$$

From the bar diagram, see Fig. 2, it can be concluded that, the statistical parameter (R) is more sensitive to the variation of A_1 (defect size) than A_2 and A_3 . Fig. 2 shows that by increasing the defect size statistical parameter (R) decreases.

5.1. Case study I: effect of incipient fault on AE statistical parameters

From Table 5 and Fig. 3, it can be concluded that AE skewness is the most appropriate and sensitive parameter for detecting incipient faults on the outer race of rolling element bearings. When condition changes from 0 mm defect to 1 mm defect all AE statistical parameters are more sensitive to the variation of defect size than rotating speed and loading condition. However skewness does not change by changing the rotating speed and loading conditions compared to other statistical parameters.

Even though, kurtosis has been used in industries as one of the most powerful statistical parameters for detecting incipient faults, it can be seen in Table 5 that kurtosis is highly sensitive to the variation of rotating speed and load. From Fig. 3 and Table 5, AE counts can be regarded as the second most sensitive parameter for detecting incipient faults on the outer race. It has to be noted that, since in many practical cases the rotating speed of the shaft is constant, burst duration and RMS are strong candidates for identifying defective rolling element bearings.

5.2. Case study II: effect of incipient faults on AE statistical parameters

From Fig. 4 and Table 6, it can be concluded that AE crest factor (CF) is the most appropriate and sensitive parameter for measuring and estimating defect size on the outer race of rolling element bearings. However, crest factor is also highly sensitive to variation of rotating speed and loading. The second most appropriate statistical parameter for diagnosing defect growth is AE counts but as it can be seen in Table 6, rotating speed has a great influence on the number of AE counts. Skewness is more sensitive to the loading conditions and by increasing the defect size, no significant change is observed. The main reason is, if there is no fault, probability density function is symmetric and skewness is close to zero. When a fault appears on a bearing, probability density function becomes asymmetric and hence skewness will change. However, by increasing the fault size, variation in the shape of probability density function of AE signals is not significant. Thus, skewness change is not high in the second case study.

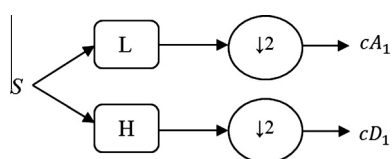


Fig. 5. Basic step of decomposition of discrete wavelet transform.

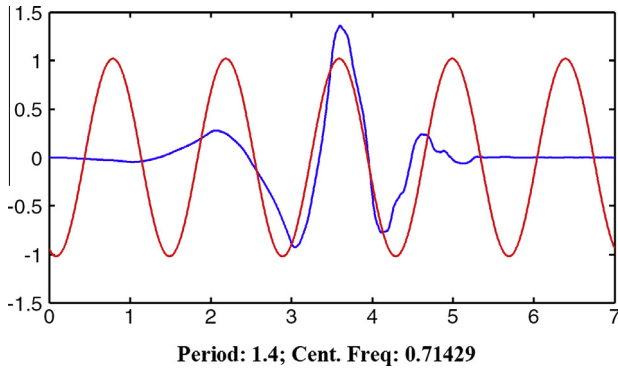


Fig. 6. Wavelet daubechies4 (blue) and center frequency based approximation. (For interpretation of the references to color in this figure legend, the reader is referred to the web version of this article.)

Table 7
Characteristics of orthogonal and biorthogonal wavelet families.

Family	Daubechies	Symmlet	Coiflets	DMeyer
Short name	db	sym	Coif	dmey
Order N	Positive integer	$N = 2, 3, \dots$	$N = 1, 2, \dots, 5$	–
Orthogonal	yes	yes	yes	yes
Biorthogonal	yes	yes	yes	yes
Compact support	yes	yes	yes	yes
DWT	Possible	Possible	Possible	Possible
CWT	Possible	Possible	Possible	Possible
Support width	$2N-1$	$2N-1$	$6N-1$	–
Filters length	$2N$	$2N$	$6N$	–

RMS and burst duration have been used as one of the most important statistical parameters for measuring defect size [16]; however, as it is illustrated in Fig. 4, RMS and burst duration can be easily distorted by changing the rotating speed of the shaft. It should be noted that in the case of constant rotating speed of the shaft, AE counts is the most promising parameter for monitoring and measuring the defect growth. Thus, for the purpose of measuring the defect size, one approach is to monitor the variation of AE counts over time. Another approach is to take advantage of

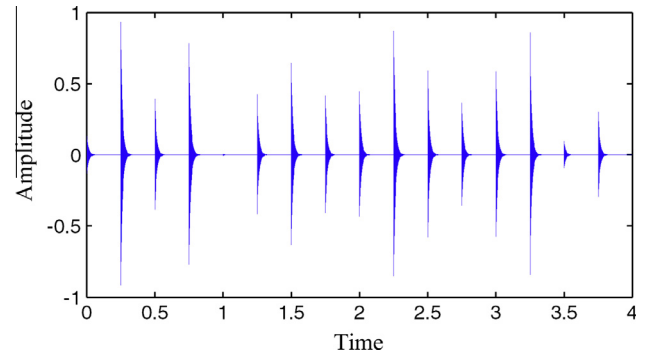


Fig. 8. Simulated impulse signal.

advanced signal processing techniques to accurately measure the defect size and its growth on different locations of rolling element bearings for estimating the fatigue life of bearings.

6. Review of WPT, Shannon entropy, and kurtogram

6.1. Wavelet packet transform

Wavelets are increasingly being used in signal processing and many engineering applications. Wavelets can be convoluted with portions of a transient signal to extract specific information from the signal at a given time. Unlike Fourier transform, which is frequency localized, continues wavelet transform (CWT) technique may be used to decompose a transient signal into series of time-domain components, each covering a specific range. Therefore, CWT has been widely used in signal processing and signal denoising due to its extraordinary time-frequency or more properly term time-scale representation capability. The continuous wavelet transform of finite-energy signals ($f(t) \in L^2(r)$) with the analyzing wavelet (mother wavelet function) $\psi(t)$, is the convolution of $f(t)$ with a scaled and conjugated wavelet:

$$W_f(a, b) = \int_{-\infty}^{+\infty} f(t) \frac{1}{\sqrt{a}} \psi^*\left(\frac{t-b}{a}\right) dt \quad (2)$$

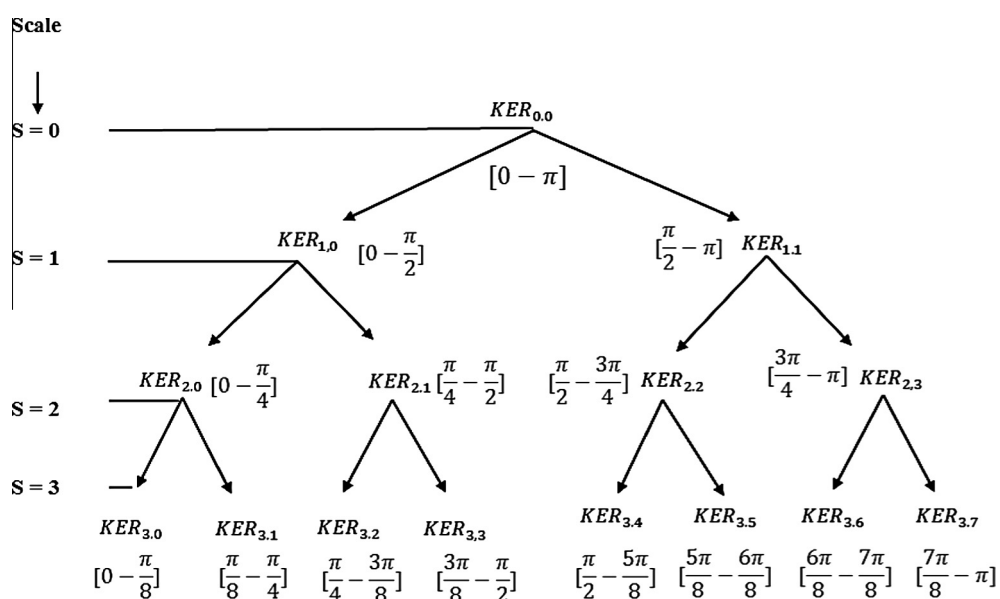


Fig. 7. Three level decomposition of wavelet packet transform (WPT).

Table 8

Simulated bearing fault parameters.

Parameters	A_i	i	F	f	α
Values	Random	16	4 Hz	2000 Hz	80

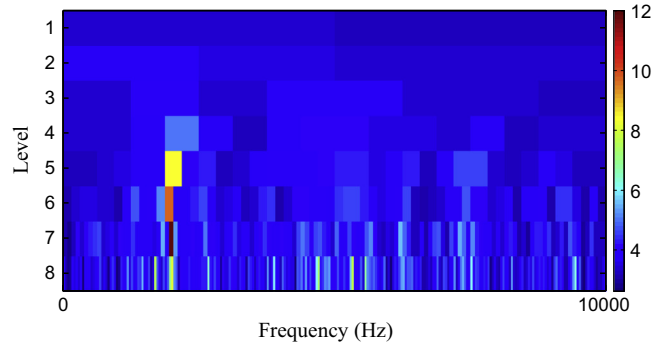
where $\psi^*(t)$ stands for the complex conjugation of $\psi(t)$. In the above Equation a and b are the dilation and translation, respectively, which may be continuous or discrete. The factor $\frac{1}{\sqrt{a}}$ is used for energy preservation. Eq. (2) indicates that the wavelet transform is a time-scale analysis. The wavelet transform can also be considered as a filtering operation by changing a and b to obtain frequency segmentation. Since in CWT method the entire frequency band of the desired signal has to be spanned by the designed wavelet function, a more efficient way of analyzing the data, is to make use of discrete wavelet transform (DWT) method. By replacing a and b with 2^{-j} and $2^{-j}k$ respectively, where k and j are integer values, the DWT can be written as:

$$W_f(j, k) = \sqrt{2^j} \int_{-\infty}^{+\infty} f(t)\psi^*(2^j t - k)dt \quad (3)$$

Discrete form of wavelet transform can be implemented by using filter $h(k)$ and $g(k)$ which are low-pass filter related to the scaling function $\phi(t)$ and high-pass filter related to wavelet function (t) , respectively.

$$\phi_j(t) = \sum_k h(k) 2^{(j+1)/2} \phi(2^{j+1}t - k) \quad (4)$$

$$\psi_j(t) = \sum_k g(k) 2^{(j+1)/2} \phi(2^{j+1}t - k) \quad (5)$$

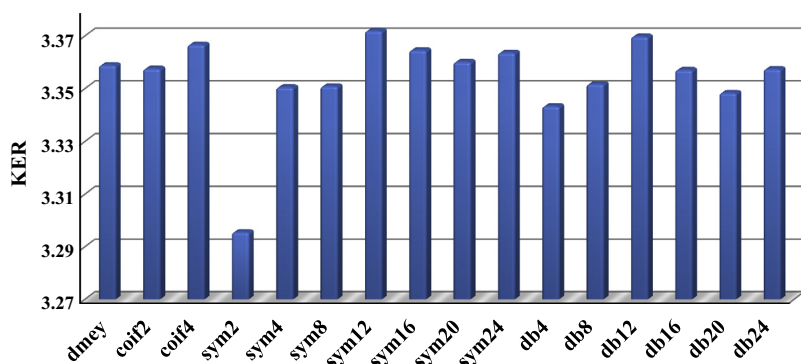
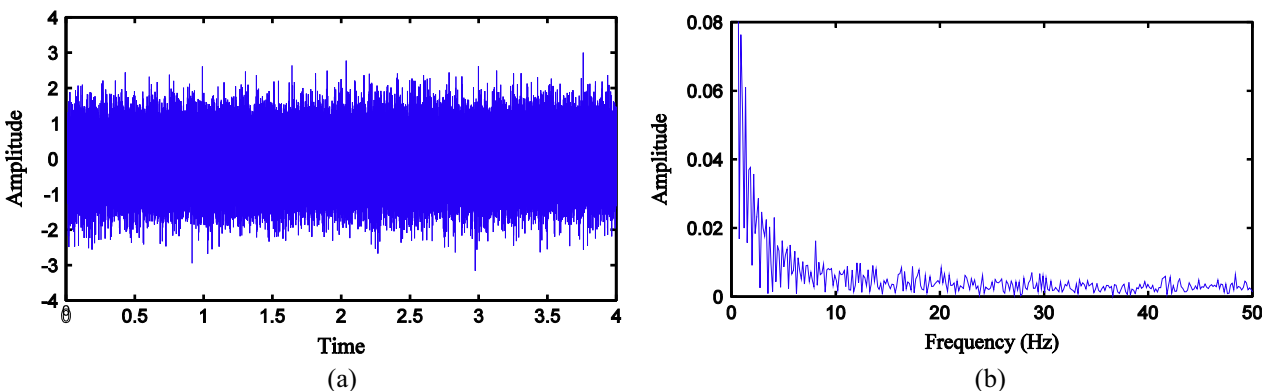
**Fig. 11.** WPT and KER calculations of the simulated bearing fault signal.

The basic step of discrete wavelet transform is illustrated in Fig. 5. The signal s is convolved with a low pass filter L and a high pas filter H . Decomposition outcomes, cA_1 and cD_1 are called approximate coefficients and detailed coefficients, respectively. The symbol $\downarrow 2$ denotes down sampling.

The wavelet packet transform (WPT) is a generalization of the DWT and it has been used in signal processing of vibration and acoustic emission signals [17]. WPT can be implemented based on wavelet filters. Thus, WPT coefficients at each level are defined by following Equations:

$$W_{j+1}^{2K} = W_j^K(n) * h(-2n) \quad (6)$$

$$W_{j+1}^{2K+1} = W_j^K(n) * g(-2n) \quad (7)$$

**Fig. 9.** Optimal wavelet selection of the simulated signal.**Fig. 10.** (a) Simulated impulse signal with noise (SNR = -22 dB), (b) envelope spectrum of the simulated signal with noise.

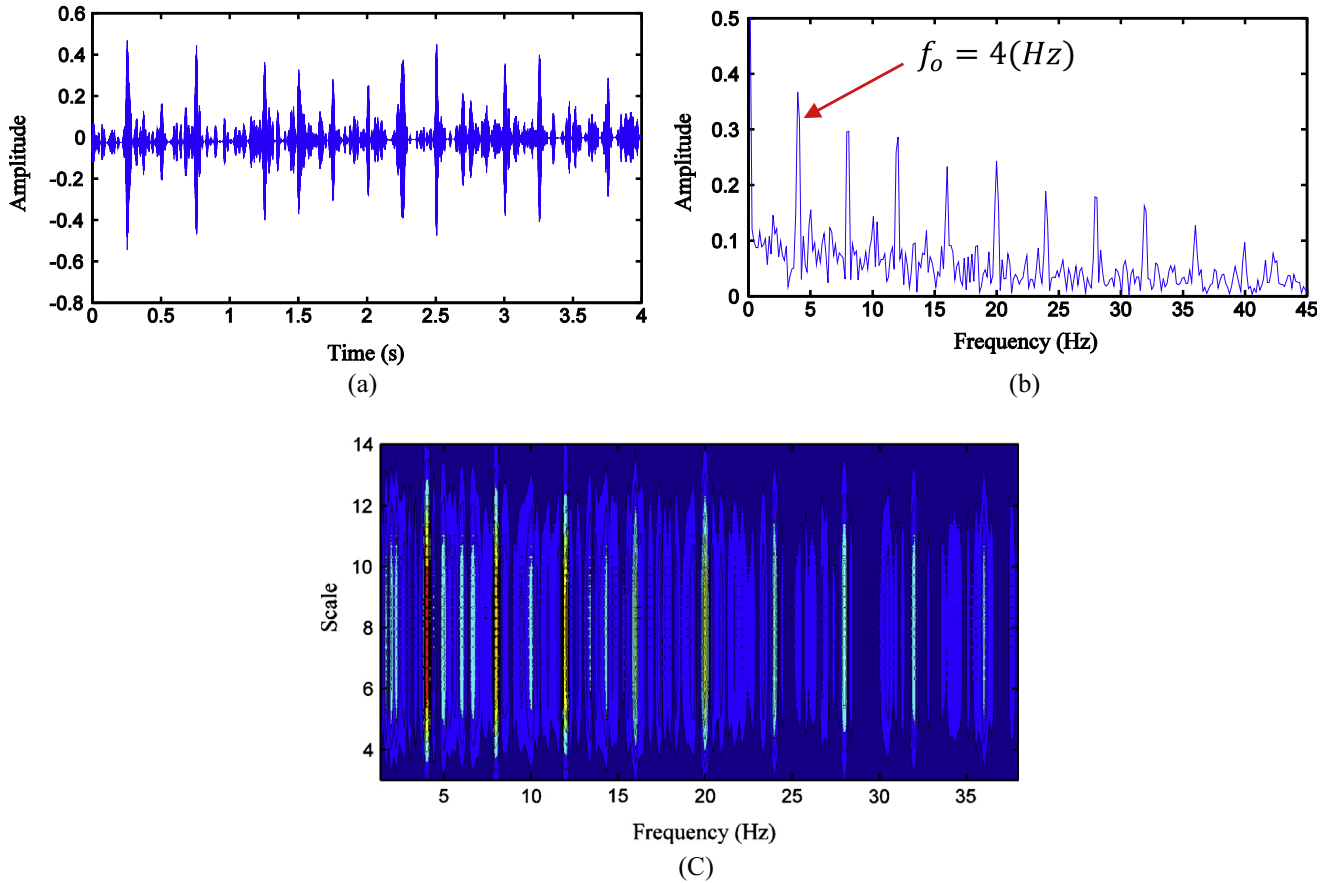


Fig. 12. (a) Frequency band signal (de-noised signal), (b) envelope spectrum of de-noised signal, (c) multiscale spectrum of de-noised signal.

where W_{j+1}^{2K} denotes the j th decomposed level of wavelet packet coefficient at frequency band of $2k(0 < k < 2^j - 1)$; $h(-2n)$ and $g(-2n)$ are the low-pass and high-pass filters, respectively based on the selected wavelet function. In practice a fast algorithm is applied by splitting approximations and details into finer components. Therefore, WPT is more efficient than CWT and DWT of the time-scale analysis to describe bearing fault signal in different frequency bands of local information. The proposed method uses the WPT as a powerful tool to do orthogonal decomposition of AE signals in the whole frequency domain. As a result, WPT can process all frequency bands, especially high frequency bands, more efficiently where bearing characteristic frequencies exist.

6.2. Shannon entropy

Entropy is a common idea in many fields, especially in signal processing and condition monitoring [18,19]. Adding small noise to a signal will cause a significant change in the value of entropy. Shannon entropy H of a discrete random variable X with possible values $\{x_1, x_2, \dots, x_n\}$ can be written as [10,20]:

$$\text{Entropy}(X) = H(x) = - \sum_{i=1}^n p(x_i) \log_2(p(x_i)) \quad (8)$$

where p is the probability mass function of a random variable X , and it can be written as energy probability distribution of a discrete signal x :

$$p(x_i) = \frac{(x_i)^2}{\sum_{i=1}^N (x_i)^2} \quad (9)$$

with the following two conditions:

$$\begin{cases} \sum_{i=1}^n p(x_i) = 1 \\ \text{if } p(x_i) = 0 \rightarrow p(x_i) \log_2(p(x_i)) = 0 \end{cases} \quad (10)$$

From Eqs. (8)–(10) it can be concluded that the Shannon entropy of a discrete signal is limited by:

$$0 \leq \text{Entropy}(x) \leq \log_2(N) \quad (11)$$

where N is the length of the discrete signal. It should be noted that, entropy of a signal will be zero if all data points are zero except for one data, and it will be $\log_2(N)$ if the probability of energy distribution of all data is equal to $1/N$. Thus, the lower the Shannon entropy the higher the concentration of energy will be. In information theory or statistical measurement, Shannon entropy is sometimes referred to as a measure of information loss of a random variable [21]. Shannon entropy of a normalized signal measures the amount of randomness and sparseness of data. Thus, a signal with minimal amount of Shannon entropy can be treated as the most periodic and greatest amount of signal to noise ratio. In the present study Shannon entropy has been used as a measure of periodicity and energy concentration of a signal in different frequency bands. When roller elements pass over a defect on bearing components, a series of AE impulses will be generated. These impulses repeat at a specific frequency, hence, the signal frequency band produced by WPT which has the minimum value of entropy contains the maximum periodicity, signal to noise ratio, and energy concentration.

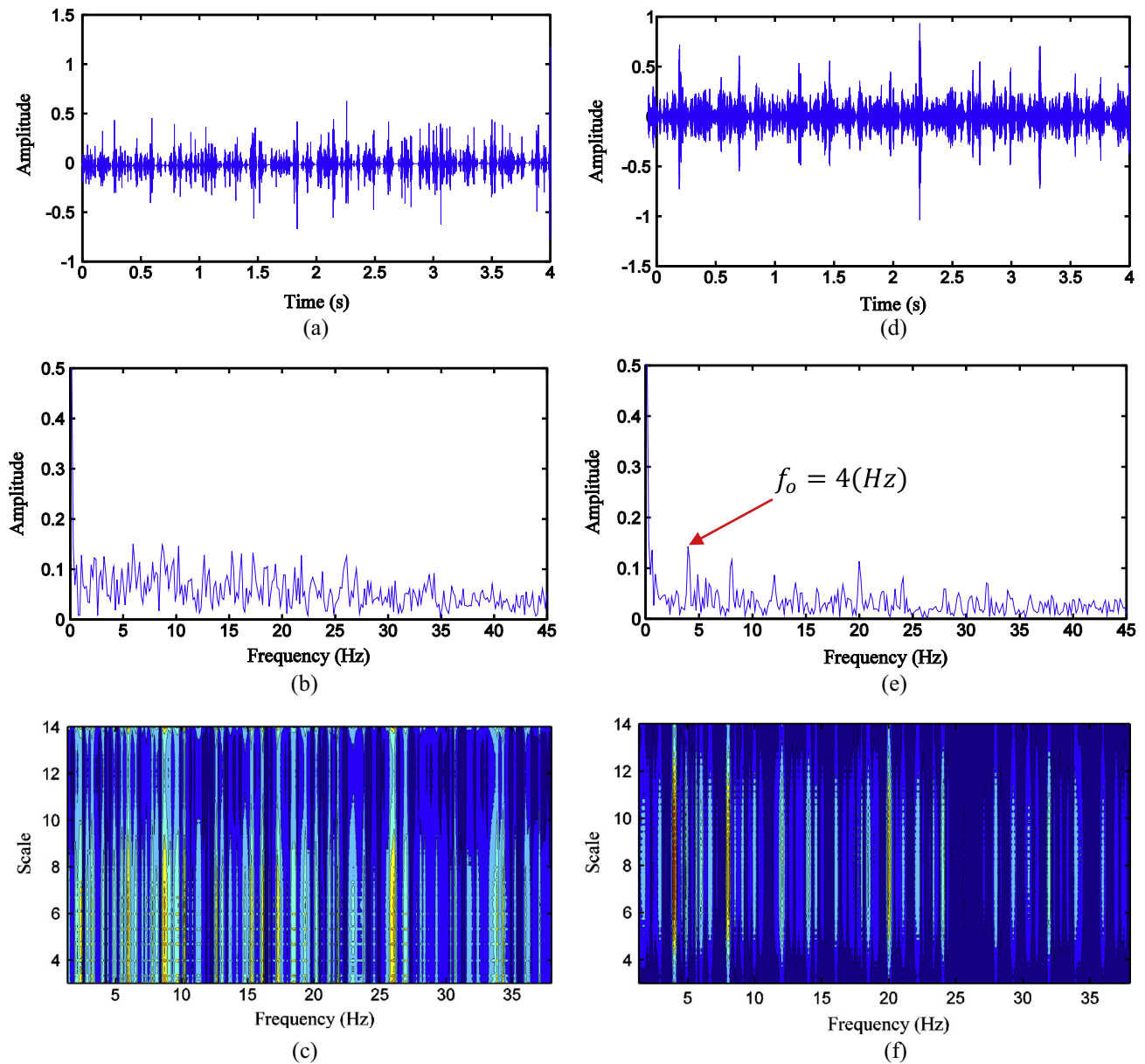


Fig. 13. (a) De-noised signal using sym2, (b) EV using sym2, (c) MSES using sym2, (d) De-noised signal using db4, (e) ES using db4, (f) MSES using db4.

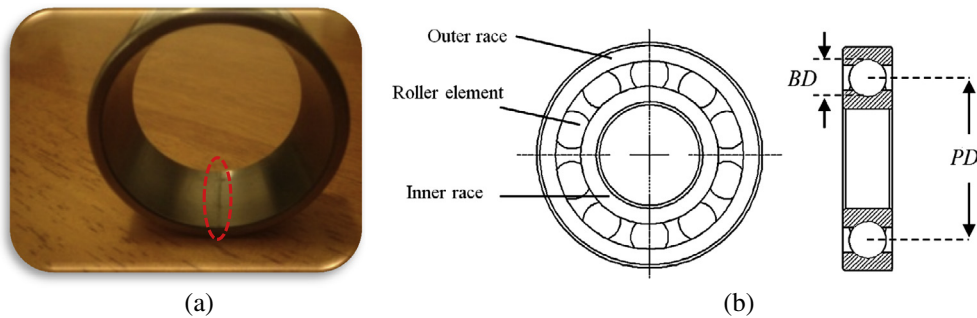


Fig. 14. (a) Picture of a line shape defect on the outer race, (b) rolling element bearing components.

Table 9

Experimental matrix for bearing characteristic frequency detection on the outer race

Condition	Rotating speed (rpm)	Load (N)
S1, L0	300	0
S1, L2	300	200
S4, L0	2200	0
S4, L2	2200	200

6.3. Kurtogram

Kurtosis characterizes the relative peakedness or flatness of a distribution of measured values. A high kurtosis distribution has a sharper peak and longer tail; however, low kurtosis distribution has smoother and curvier peak and thinner tail. Kurtosis has been used as a measure of the severity of machine faults since it was introduced by Dyer & Stewart [6].

$$\text{Kurtosis} = \frac{(N) \sum_{i=1}^N (x_i - \bar{x})^4}{\left(\sum_{i=1}^N (x_i - \bar{x})^2 \right)^2} \quad (12)$$

Spectral kurtosis (SK) was first used by Dwyer [22] for detecting impulsive events in sonar signals. It was based on the short time Fourier transform (STFT) and measures impulsiveness of a signal as a function of frequency. Also, SK has been used to identify the presence of non-Gaussian components due to bearing faults and to indicate in which frequency range it may occur. This may be utilized to discover the presence of transients in a signal and for finding their locations in the frequency domain. A thorough review of the subject and its application to condition based health monitoring and machine fault diagnosis may be found in [23]. Based on Wold-Cramér decomposition of a non-stationary signal, the signal $X(t)$, as

a response of a system, for the case of a series of impulses $h(t)$, which can be a model of a rolling element bearing signal, excited by $Z(t)$ can be written as [23],

$$X(t) = \int_{-\infty}^{+\infty} e^{j2\pi ft} H(t,f) dZ(f) \quad (13)$$

where $dZ(f)$ is an orthonormal spectral increment and $H(t,f)$ is the complex envelope of $X(t)$ at frequency f . The SK can be defined by taking the fourth power of $H(t,f)$ at each time and averaging its value along the record and normalizing it by the square of the mean square value. It can be proved that if 2 is subtracted from this ratio, as given in Eq. (14), the result will be zero for a Gaussian signal [23]:

$$K(f) = \frac{\langle H^4(t,f) \rangle}{\langle H^2(t,f) \rangle^2} - 2 \quad (14)$$

Spectral kurtosis (SK) is proved as an effective tool which can locate frequency bands with a high amount of impulsiveness, and also for filtering out the signal to maximize peakendness. Thus, kurtosis will be high if the filtered signal has separated impulses which can be regarded as bearing characteristic frequency. Antoni [23] computed the STFT-based SK for different window lengths to calculate the window length which maximizes the overall level of the SK in the selected frequency band. This technique was investigated in detail, and led to the concept of the “kurtogram”, which is a two dimensional map and presents optimum central frequency (f) and bandwidth (Δf) where kurtosis value is maximum. The problem of this technique is kurtogram does not provide any information regarding periodicity of a signal at each frequency band. A detailed information and fast computational of kurtogram is presented in [24].

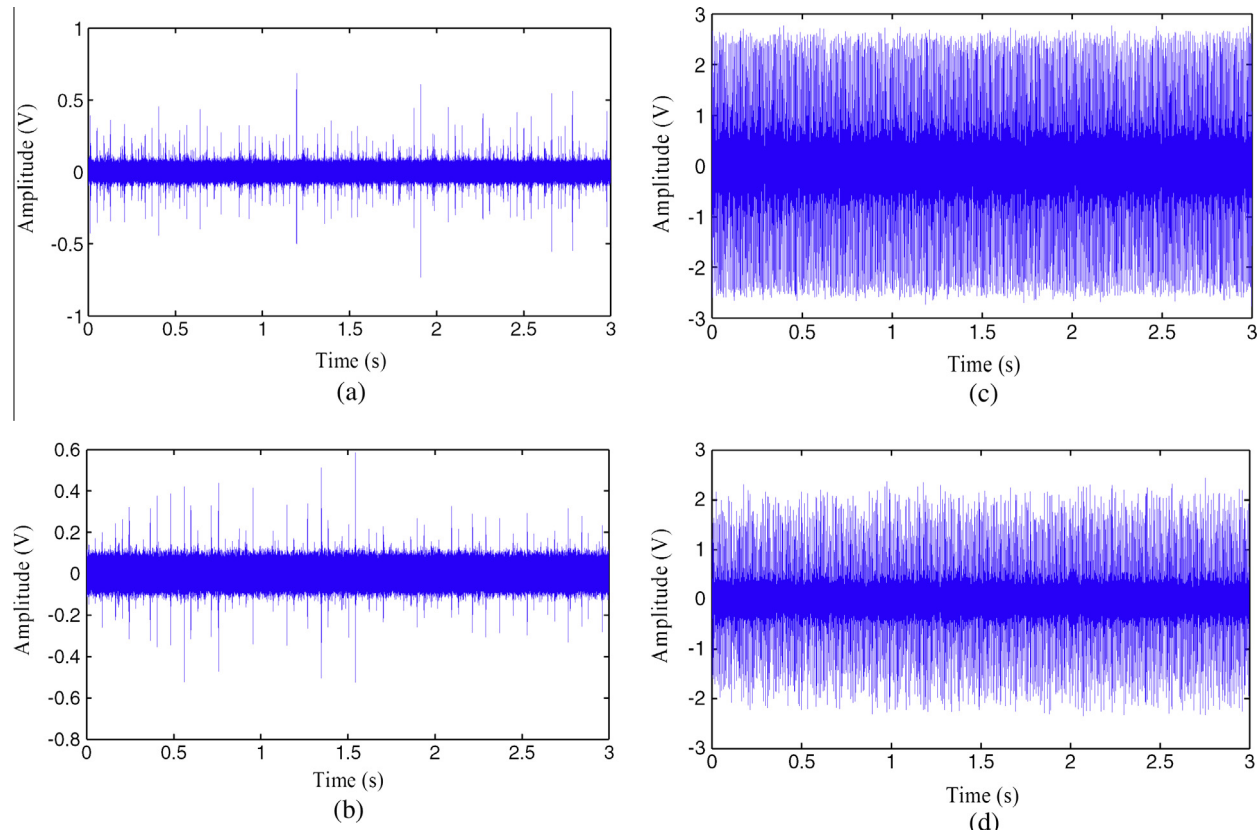


Fig. 15. AE signals from the bearing with an outer race line shape defect, (a) condition (S1, L0), (b) condition (S1, L2), (c) condition (S4, L0), and (d) condition (S4, L2).

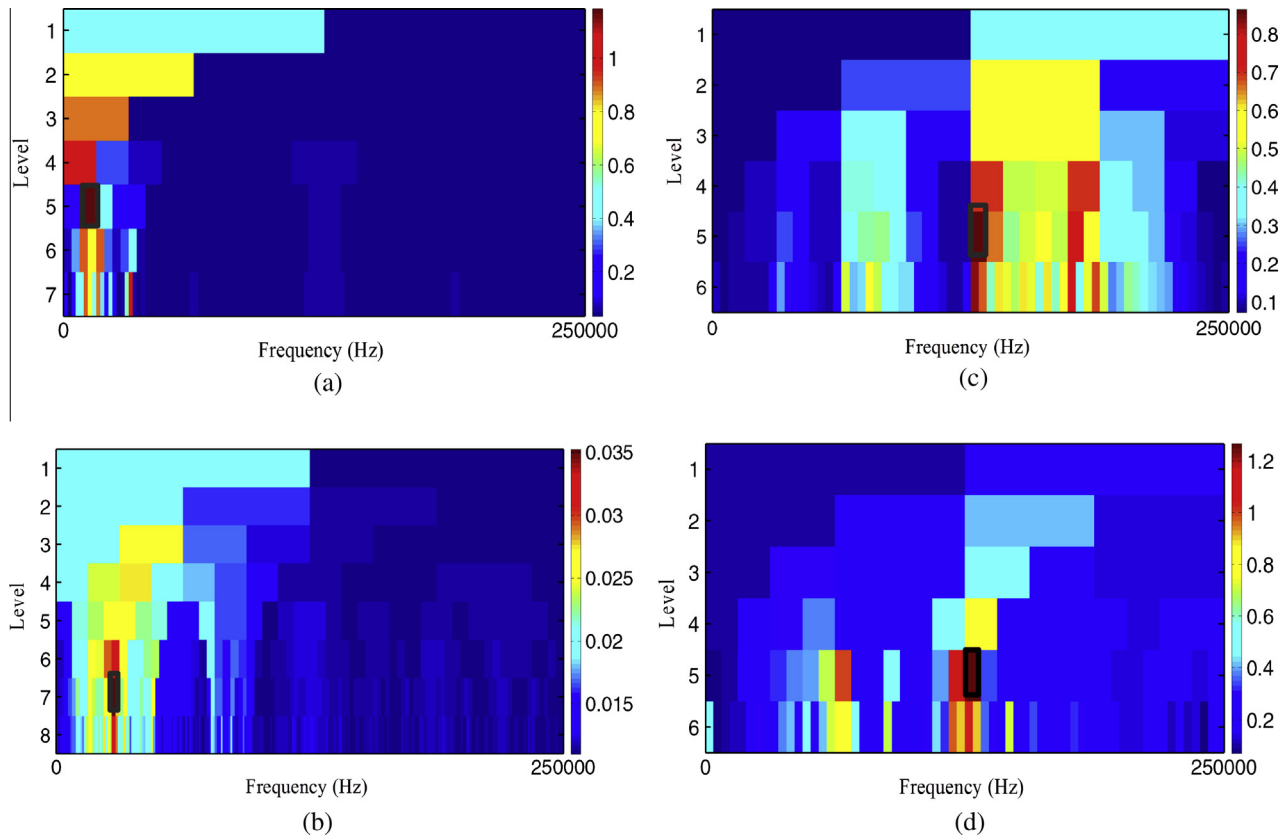


Fig. 16. WPT and KER calculations of AE signals, (a) condition (S1, L0), (b) condition (S1, L2), (c) condition (S4, L0), and (d) condition (S4,L2).

$$\hat{x}(t) = \frac{1}{\pi t} * x(t) = \frac{1}{\pi} \int_{-\infty}^{+\infty} \frac{x(\tau)}{t - \tau} d\tau \quad (15)$$

By coupling the $x(t)$ and $\hat{x}(t)$, analytical signal $h(t)$ can be calculated as,

$$h(t) = x(t) + j\hat{x}(t) = a(t)e^{i\varphi(t)} \quad (16)$$

where $a(t)$ is the envelope of the signal

$$a(t) = \sqrt{x^2(t) + \hat{x}^2(t)}, \quad \varphi(t) = \arctan(\hat{x}(t)/x(t)) \quad (17)$$

7. Optimal mother wavelet selection for bearing fault diagnostics using continuous wavelet transform (CWT)

A critical issue to ensuring the effectiveness of continuous wavelet transform and discrete wavelet transform in rolling element bearing fault diagnosis is the choice of the most appropriate mother wavelet for signal decomposition and feature extraction. Many researchers have attempted to tackle the issue of optimal mother wavelet selection. For example, Shape matching has been used for selecting the optimal mother wavelet to determine the impulses in vibration signals [26]. However, it is not always possible to visually match the shape of the signal to that of the mother wavelet. Maiming the cross correlation function has also been used as a technique for optimal wavelet selection in ECG signals [27], but signals which are buried in high level of noise cannot be detected utilizing cross correlation function.

To solve this issue a quantitative measurement tool is used to select the optimal mother wavelet for analyzing the measured acoustic emission signals. In this work, a quantitative measurement is proposed and utilized. The measurement is based on continuous wavelet transform and kurtosis-to-Shannon entropy ratio.

Table 10

Optimal wavelet function and frequency bands under different conditions.

Condition	Optimal wavelet function	Optimal frequency band (Hz)	Level
S1, L0	db39	7812.5–15,625	5
S1, L2	db44	27343.75–29296.875	7
S4, L0	sym24	125,000–132812.5	5
S4, L2	db22	125,000–132812.5	5

6.4. Hilbert transform

The acoustic signals of interest have repetitive high frequency impulses as a consequence of interaction between rolling element components and defects. These burst sounds generated by the bearing defects are modulated in amplitude by the sequence of repetitive impacts and by the damping effect. The direct FFT analysis of the signals does not provide much information, since noise and high frequency components caused by movement of rolling elements against each other will be mixed with the characteristic frequencies of bearing faults. These repeating fault frequencies are, however, easily measured in the signal envelope. The envelope detection method provides an important and effective approximation to analyze fault signals in high frequency vibrations. The signal envelope can be calculated by the Hilbert transform [25] which acts as a linear operator on the signal to produce a function with the same domain. Given a signal $x(t)$ in the time domain, the Hilbert transform is the convolution of $x(t)$ with the signal $\frac{1}{\pi t}$ which produces a new signal in the time domain. Hilbert transform can be defined as:

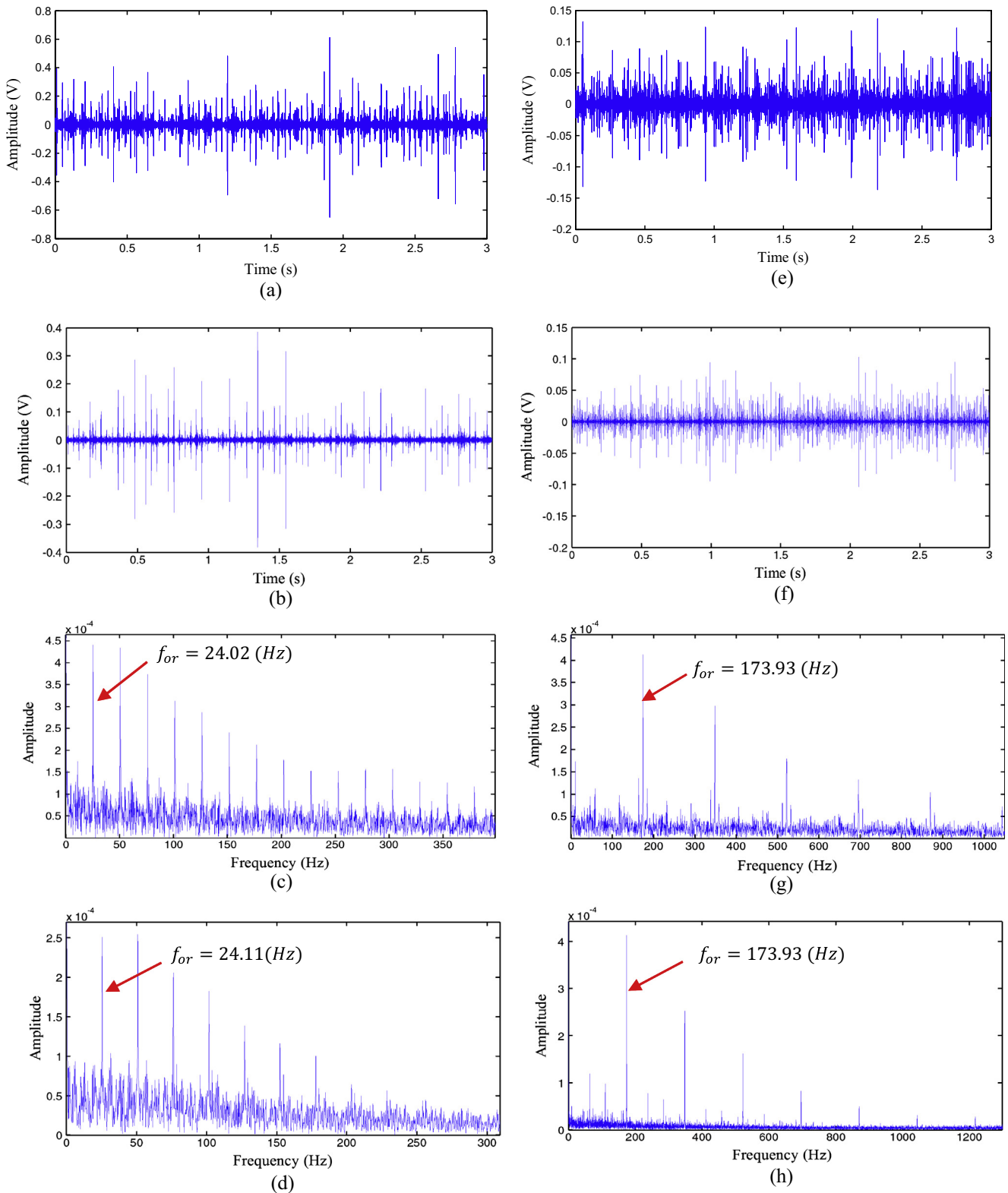


Fig. 17. De-noised AE signals and their envelope spectrum, (a), and (c) condition (S1, L0), (b), and (d) condition (S1, L2), (e), and (g) condition (S4, L0), (f), and (h) condition (S4, L1).

Both the simulated bearing fault signal and an actual roller element bearing AE signal have been used to evaluate the effectiveness of the developed measure on mother wavelet selection.

Analytical and experimental results demonstrate that the mother wavelet selected based on the proposed algorithm presents an optimal mother wavelet in diagnosing bearing defects.

Table 11

Characteristic fault frequency analysis for the outer race line defect shape under different conditions.

Condition	Theoretical frequency (Hz)	Measured frequency (Hz)	Error (%)
S1, L0	23.62	24.02	1.7
S1, L2	23.62	24.11	2
S4, L0	173.21	173.93	0.4
S4, L2	173.21	173.93	0.4

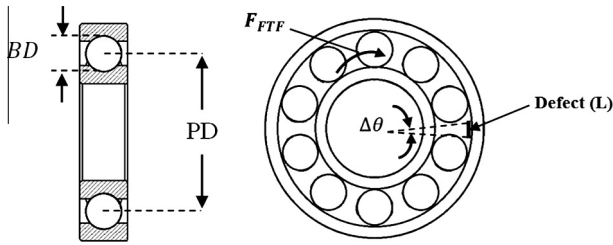


Fig. 18. Schematic of rolling element bearing components with an outer race defect.

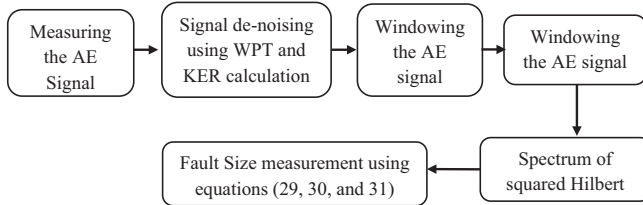


Fig. 19. Flow chart of defect size estimation.

7.1. Kurtosis to Shannon entropy ratio (KER) calculation

The kurtosis of a discrete signal can be calculated in the wavelet domain from its corresponding continuous wavelet transform coefficients and may be expressed as:

$$\text{Kurtosis} = \frac{(N) \sum_s \sum_n (C(s, n) - \bar{C}(s, n))^4}{\left(\sum_s \sum_n (C(s, n) - \bar{C}(s, n))^2 \right)^2} \quad (18)$$

Based on the above Equation kurtosis value associated with a particular scaling parameter s is expressed as:

$$\text{Kurtosis}(s) = \frac{(N) \sum_{i=1}^N (C(s, n) - \bar{C}(s, n))^4}{\left(\sum_{n=1}^N (C(s, n) - \bar{C}(s, n))^2 \right)^2} \quad (19)$$

where N is the number of wavelet coefficients at each scale, and $C(s, n)$ is the wavelet coefficients at scale s . When applying wavelet transform to a signal, if a major frequency component corresponding to a particular scale s exists in the signal, then the wavelet coefficients at that scale will have relatively high value of kurtosis and more impulses in time domain. For purpose of bearing health diagnosis, the higher the kurtosis content extracted from defective bearing is, the more effective the selected base wavelet will be. Thus the maximum kurtosis information can be used as a measure for the optimal mother wavelet selection. Furthermore, given that for the same amount of kurtosis within a frequency-band signal, the peri-

odicity of impulses and energy concentration may be significantly different. The spectral concentration of the energy and periodicity of impulses need also to be considered to ensure effective extraction of the defect-induced transient AE burst. According to Eqs. (8) and (9) the energy distribution of the wavelet coefficients can be quantitatively described by the Shannon entropy as [28]:

$$\text{Entropy}(s) = - \sum_{i=1}^N \frac{|C(s, n)|^2}{\sum_{n=1}^N |C(s, n)|^2} \cdot \log_2 \left(\frac{|C(s, n)|^2}{\sum_{n=1}^N |C(s, n)|^2} \right) \quad (20)$$

where N is the number of wavelet coefficients at each scale, and $C(s, n)$ is the wavelet coefficients at scale s . By examining the wavelet coefficients that represent the defect-induced transient AE burst, an appropriate base wavelet should extract the maximum amount of kurtosis while minimizing the Shannon entropy of the corresponding wavelet coefficients. A combination of the kurtosis and Shannon entropy content of a signal's wavelet transform coefficients, denoted as kurtosis-to-Shannon entropy ratio (KER), can thus be designed as:

$$\text{KER}(s) = \frac{\text{Kurtosis}(s)}{\text{Entropy}(s)} \quad (21)$$

where the Kurtosis(s) and Entropy(s) are calculated using Eqs. (19) and (20), respectively. Accordingly, the appropriate base wavelet can be selected from a set of base wavelets by maximizing the kurtosis to Shannon entropy ratio (KER(s)). The mother wavelet that has produced the maximum kurtosis to Shannon entropy ratio is chosen to be the most fitting wavelet for bearing fault extraction. To analyze the test signal using various orthogonal wavelets, the scale whose corresponding center frequency is equal to that of interest (the frequency which has the maximum amplitude from spectral analysis) is chosen to perform the wavelet transform. In general, scale s and its corresponding frequency of a mother wavelet function (F_a) with a central frequency of F_c are related by [29]:

$$F_a = \frac{F_c}{s \times \Delta} \quad (22)$$

where Δ is the sampling period and F_a is the pseudo-frequency corresponding to the scale s . Fig. 6 illustrates the procedure of calculating the central frequency of mother wavelet Daubechies4 function.

8. The proposed method and its application

Local defects on the roller element bearing components cause periodic impulses in AE signals. AE impulses can be masked and distorted by the background noise. Thus, the frequency band which contains a signal with maximum periodicity and signal to noise ratio can be regarded as the optimal band-pass filter. In this study:

- Best wavelet function is selected using the CWT and KER calculation. Thus, wavelet coefficients are calculated utilizing 4 orthogonal mother wavelet families which are DMeyer, Daubechies, Symlets, and Coiflets to investigate which wavelet function maximizes its corresponding KER value. Characteristics of orthogonal and biorthogonal wavelet families are tabulated in Table 7.
- The wavelet packet transform is implemented on the acoustic emission (AE) signal, and thus, different frequency-band signals are produced according to the WPT decomposition level.
- Envelope of AE signals in different frequency bands is calculated using Hilbert-transform.
- The value of kurtosis to entropy ratio (KER) is calculated for each of envelopes from WPT frequency-bands. The WPT decomposition of a signal with a sampling frequency of 2π utilizing kurtosis to Shannon entropy (KER) for three level of decomposition is shown in Fig. 7.

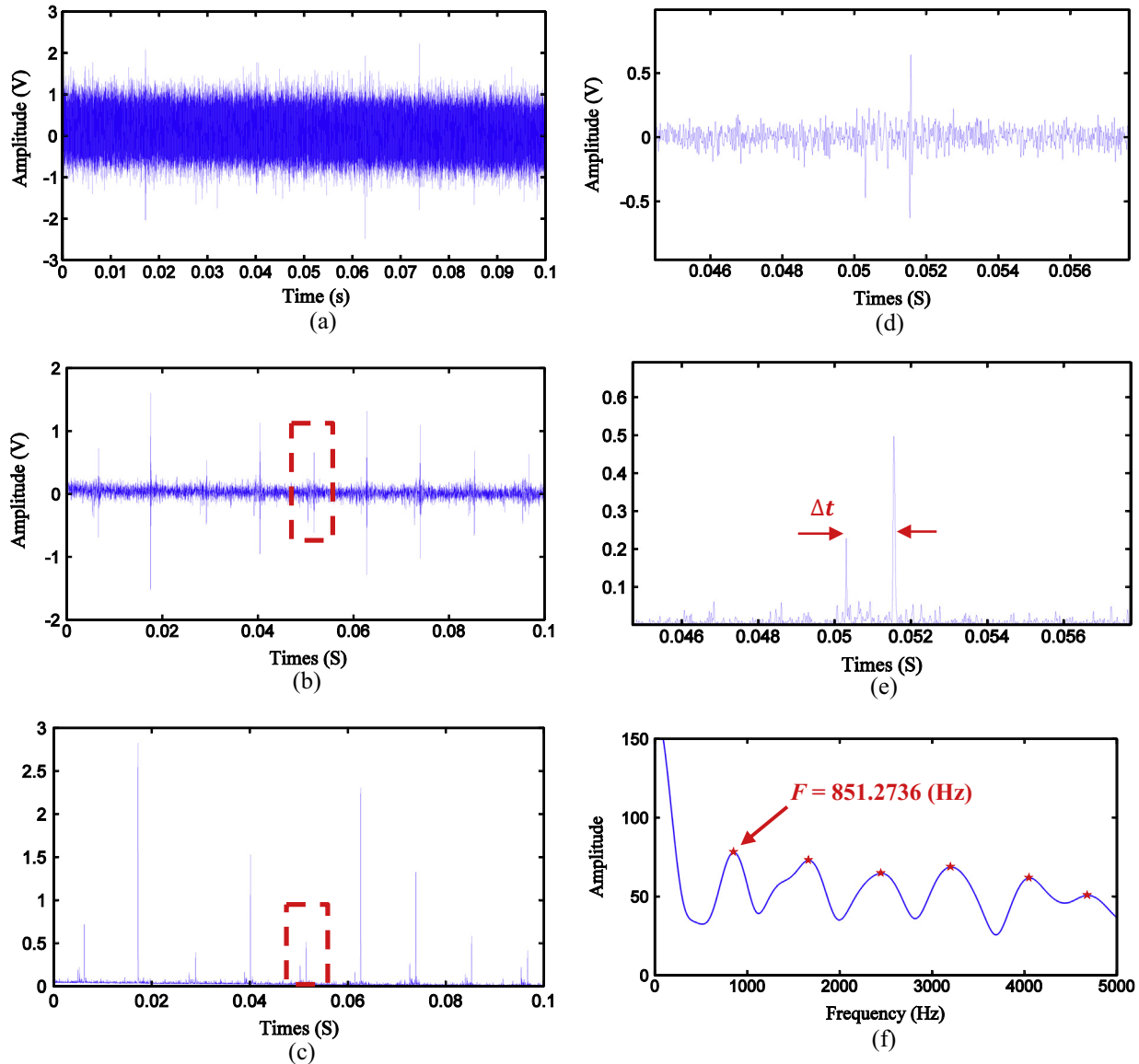


Fig. 20. (a) AE signal under condition (Outer Race, S3, L1, D1), (b) de-noised AE signal using the proposed method and mother wavelet db22, (c) squared Hilbert transform of de-noised signal, (d) windowed AE signal, (e) squared Hilbert transform of windowed AE signal, (f) zero-padded spectrum of squared Hilbert transform of windowed AE signal.

- Frequency band which has the maximum value of KER is selected as an optimal band-pass filter since it contains characteristic fault frequencies.
- De-noising the band-passed signal using adaptive thresholding method given by Eq. (23).

$$thr = \sqrt{2 \times \ln(n)} \times s \quad (23)$$

where n is the length of the discrete signal and s is an estimate of noise level [30].

- Envelope spectrum using Hilbert transform along with FFT is constructed to diagnose characteristic defect frequencies of faulty bearing.
- Multi-scale analysis for better resolution in frequency domain.

The flow chart of the proposed method is shown in Fig. 7. As mentioned above optimal frequency-band signal is selected based on:

- High sensitivity of kurtosis value to impulses which are attributed to AE pulses caused by movement of rolling element components over localized defects.
- High sensitivity of Shannon entropy to fault periodic pattern, signal to noise ratio, and energy concentration in the measured signals.

Therefore the proposed method can simply extract a band-pass filtered signal, even with small signal to noise ratio, which contains fault features.

8.1. Feature extraction of the simulated signal utilizing the proposed method

In order to observe the effectiveness of the proposed method, this method is applied to a sample of simulated data. Simulated data from [31] with simple modification is used to simulate faulty bearings. Simulated signal is illustrated in Fig. 8.

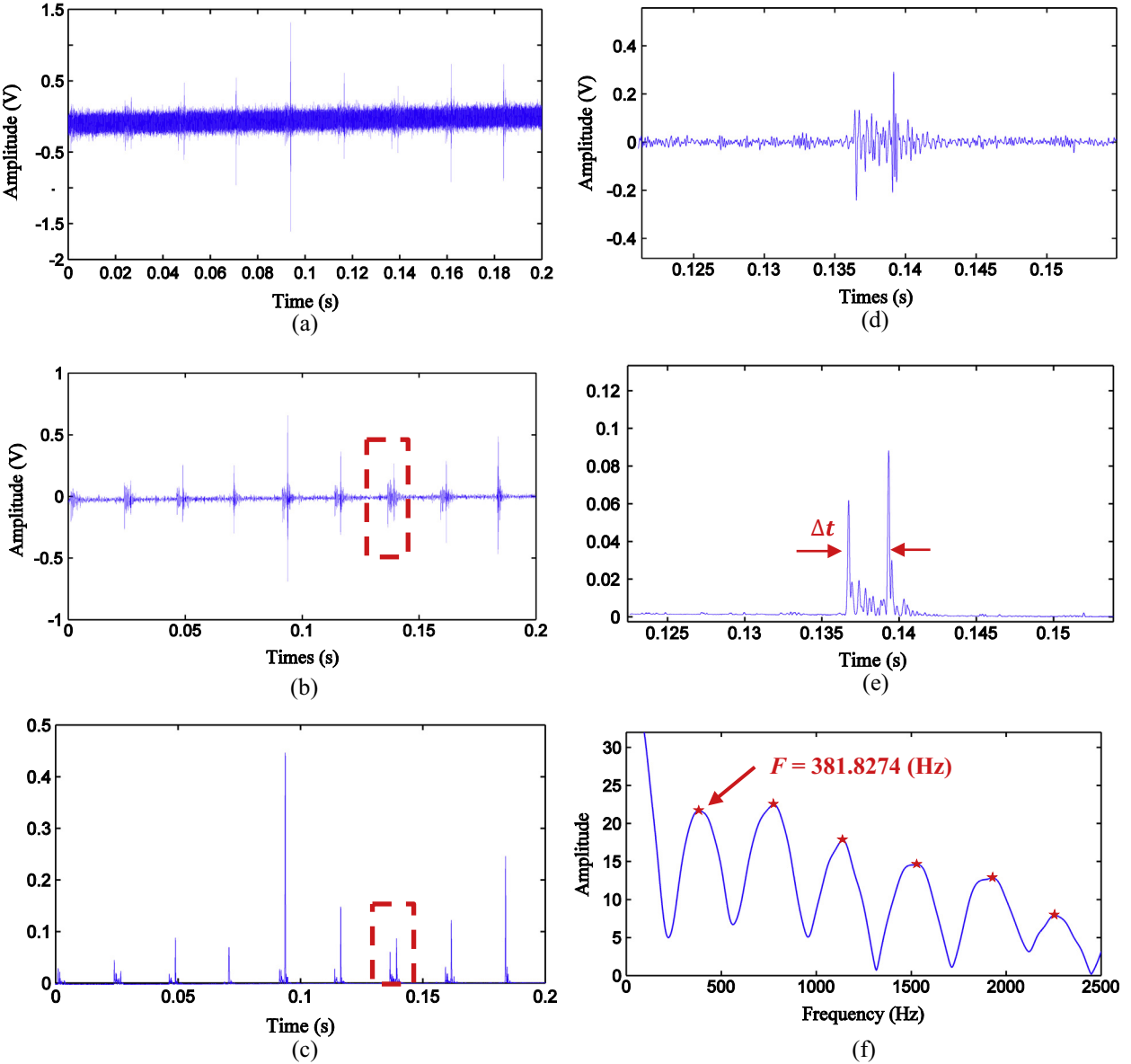


Fig. 21. (a) AE signal under condition (Rolling Element, S2, L0, D1), (b) de-noised AE signal using the proposed method and mother wavelet sym24, (c) squared Hilbert transform of de-noised signal, (d) windowed AE signal, (e) squared Hilbert transform of windowed AE signal, (f) zero-padded spectrum of squared Hilbert transform of windowed AE signal.

$$g_i(t) = \begin{cases} A_i e^{-\alpha(t-\frac{i}{f})} \sin(2\pi f(t - \frac{i}{f})) & \text{if } (t - \frac{i}{f}) > 0 \\ 0 & \text{if } (t - \frac{i}{f}) < 0 \end{cases} \quad (24)$$

where A_i is amplitude of i th impulse and N is number of impulses which is assumed to be random. F , f , and α are the characteristic fault frequency, excited resonance frequency and decay parameter, respectively. Simulated signal can be written as:

$$S(t) = \sum_{i=1}^N g_i(t) + Z(n) \quad (25)$$

where $g_i(t)$ is i th impulse and $Z(n)$ is Gaussian white noise which is added to the original data to produce a noisy signal of $S(t)$. In this paper, sampling frequency and characteristic fault frequency of a simulated signal of faulty bearing are set to 20 kHz and 4 Hz, respectively, and all parameters are given in Table 8.

To examine the performance of the proposed method, signal to noise ratio of -22 dB is selected; see Fig. 10(a), to simulate an

extremely noisy bearing fault signal. From the envelope spectrum of the noisy signal shown in Fig. 10(b) no information can be obtained. It is observed that defect frequency is completely masked by noise. This means that the envelope spectrum fails to extract characteristic frequencies from a noisy signal. Wavelet selection method is applied to diagnose the best wavelet function. Fig. 9 illustrates the bar diagram of the KER value of different mother wavelet families.

Symmlet wavelet (sym12) is selected as the best mother wavelet function which maximizes the KER of wavelet coefficients. Then the proposed method is implemented using WPT along with KER calculation of each frequency band signal to detect the optimal band-pass filter which is shown in Fig. 11. It is shown that the maximum value of KER is at the seventh decomposition level which is node number 148 of WPT tree. The band-passed signal which is shown in Fig. 12(a) reveals clear impulses. Characteristic frequency of 4 Hz and its harmonics are obvious from the envelope spectrum of frequency band signal in Fig. 12(b). Fig. 12(c) shows

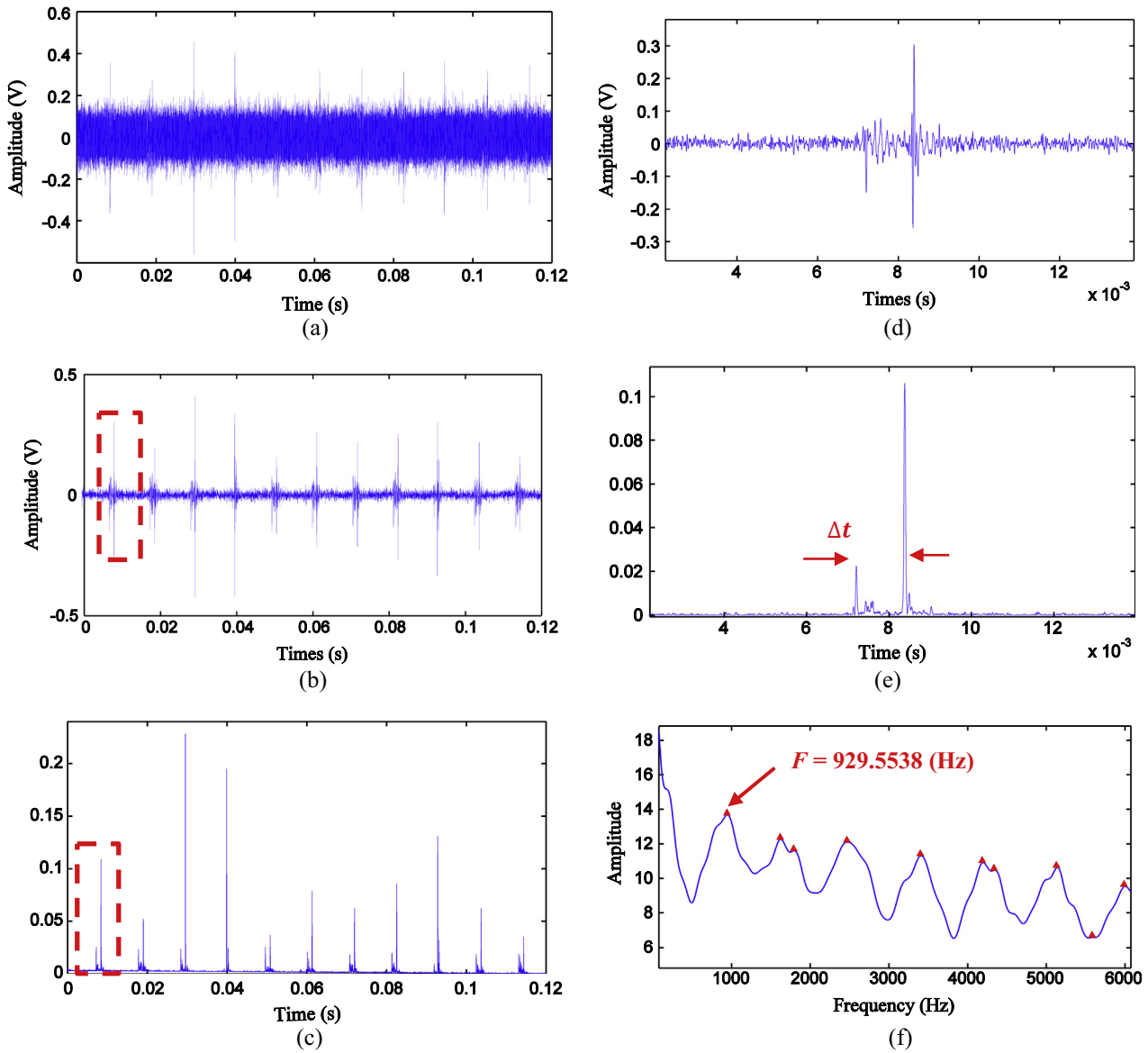


Fig. 22. (a) AE signal under condition (Inner Race, S3, L0, D1), (b) de-noised AE signal using the proposed method and mother wavelet db39, (c) squared Hilbert transform of de-noised signal, (d) windowed AE signal, (e) squared Hilbert transform of windowed AE signal, (f) zero-padded spectrum of squared Hilbert transform of windowed AE signal.

Table 12

Outer race estimated defect size under different conditions for line defect shape.

Speed (rpm)	Defect size (mm)	Estimated defect size (mm)		Error %	
		L0	L1	L0	L1
(s2)600	1	1.016	1.023	1.6	2.3
(s3)1100	1	1.062	1.084	6.2	8.4
(s2)600	2	2.044	2.104	2.2	5.2
(s3)1100	2	2.064	2.132	3.2	6.6

multi-scale enveloping spectrum (MSES) of the de-noised signal for better resolution in frequency domain [32]. MSES algorithm decomposes the discrete signal into different scales using continuous wavelet transform (CWT).

After decomposition, the envelope spectrum of signals in each scale is calculated utilizing Hilbert transform along with FFT. Thus, the final output is a three-dimensional scale-frequency color map that indicates the intensity and frequency of the defect. The

Table 13

Rolling element estimated defect size under different conditions for line defect shape.

Speed (rpm)	Defect size (mm)	Estimated defect size (mm)		Error %	
		L0	L1	L0	L1
(s2) 600	1	1.085	1.074	8.5	7.4
(s3) 1100	1	1.054	1.073	5.4	7.3
(s2) 600	2	2.064	2.131	3.2	6.5
(s3) 1100	2	2.098	2.133	4.9	6.6

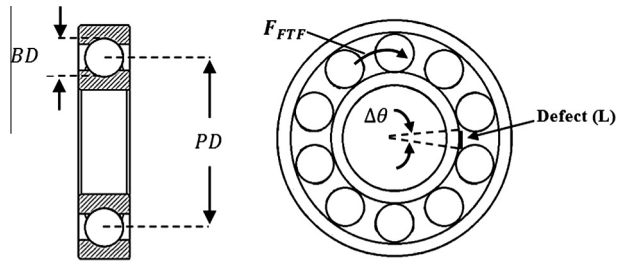
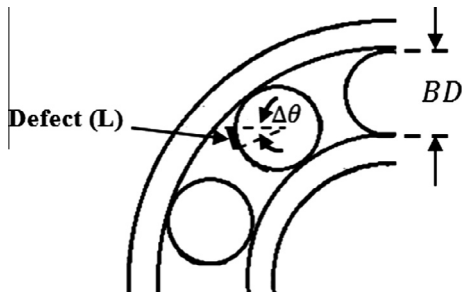
multi-scale enveloping spectrogram algorithm combines the advantages of time-scale and frequency domain features and provides more information on the defect feature. To analyze the noisy signal using MSES algorithm, the wavelet decomposition scales are chosen from 3 to 14 with an increment of 0.05, which cover the frequency range from 1020 Hz to 4800 Hz.

To compare the effectiveness of the proposed method in selecting the optimal mother wavelet function and its effect on fault

Table 14

Inner race estimated defect size under different conditions for line defect shape.

Speed (rpm)	Defect size (mm)	Estimated defect size (mm)		Error %
		L0	L1	
(s2)600	1	1.016	1.023	1.6 2.3
(s3)1100	1	1.062	1.084	6.2 8.4
(s2)600	2	2.044	2.104	2.2 5.2
(s3)1100	2	2.064	2.132	3.2 6.6

**Fig. A.1.** Schematic of rolling element bearing components with an inner race defect.**Fig. A.2.** Schematic of bearing components with a roller element defect.

diagnosis, sym2 and db4, first lowest and the second lowest value of KER in Fig. 9, are selected to extract the fault features. As it is illustrated in Fig. 13(b), and (c), there is no peak at defect frequency (4 Hz) in which the selected sym2 wavelet is used as the mother wavelet. For db4 mother wavelet, see Fig. 13(e), and (f), characteristic frequency of 4 Hz and its harmonics are not as obvious as extracted frequencies using sym12, Fig. 12(b). For purpose of comparison, it is seen that selection of the appropriate mother wavelet function is important in feature extraction and signal de-noising of impulse like signals. This verifies the effectiveness of the kurtosis-to-Shannon entropy ratio (KER) measure on wavelet selection for feature extraction in rolling element bearing fault diagnostics.

8.2. Characteristic fault frequencies of a faulty roller element bearing, experimental results

The experimental tests for diagnosing the characteristic fault frequencies were carried out using a faulty bearing with an outer race line defect shape. Localized defect was seeded on the outer race. The size of the artificial line defect was 1 mm in width and 0.5 mm in depth which is shown in Fig. 14. In a faulty bearing, defects at different locations (inner race, outer race, and roller) have characteristic fault frequencies at which bursts occur. Therefore, an AE signal of a defective bearing consists of periodic events at a corresponding characteristic fault frequency. Assuming a bearing with a fixed outer race, the characteristic defect frequency of outer race can be theoretically calculated as follows [3]:

$$f_{or} = \frac{n}{2} f_s \left(1 - \left(\frac{BD}{PD} \right) \cos \beta \right) \quad (26)$$

where BD and PD are roller diameter and bearing pitch diameter, respectively. f_s is the shaft rotating speed, β is the contact angle between the outer race and the ball, and n is the number of roller elements. For speeds up to 2200 rpm, outer race defect frequencies lie in the low-frequency range (less than 200 Hz). However, in reality, due to slipping in the rolling element bearings, outer race characteristic frequency may be slightly different from its calculated value [33]. By comparing the measured characteristic frequency and the theoretical frequency, location of the defect can be identified.

For the results in this section, measured AE signals were all sampled at a rate of 500 kHz and a total number of 1,500,000 (3 s) data points were recorded. The conditions at which experiments were conducted are tabulated in Table 9. AE signals that have been acquired under different conditions are illustrated in Fig. 15. As it can be seen in Fig. 15 the intensity of AE signals increases by applying higher radial loads, while the quality of all the signals are affected by the presence of noise. The WPT along with KER calculation at each frequency band is applied on the AE signals which are shown in Fig. 16. The maximum KERs for each condition are indicated by the black rectangles. By comparing the maximum KERs at different speeds, it can be concluded that at low speeds bearing fault impulses are more localized at low frequencies, however, at high speeds they are more shifted to the high frequencies. The results for the best mother wavelet function based on CWT and maximizing the KER values and optimal band-pass filter are summarized in Table 10. The successful enhancement of the features in the AE signals can be verified by direct comparison of the results shown in Figs. 15 and 17. The envelope spectrum, using Hilbert transform, of filtered signals clearly show the bearing fault frequencies and their harmonics Fig. 17(c), (d), (g), and (h). The measured fault frequencies and their theoretical values for the outer race line defect shape are summarized in Table 11.

The maximum deviation of the measured frequencies from the calculated theoretical values does not exceed 3% error which is again an indication of the applicability and preciseness of the proposed method. Hence, the proposed method can accurately measure bearing fault frequencies on the outer race.

8.3. Defect size estimation on rolling element bearing using the proposed method with combination of spectrum of squared Hilbert transform

After successfully characterizing the fault frequencies, the new goal is to find the actual defect size by means of studying the time duration between double spikes in the measured AE signals. Epps and McCallion [34] first indicated two spikes in gearbox fault diagnosis using vibration data. They also mentioned that as the size increases the time duration between the two spikes increases for the fixed shaft speed. Thus, if each impulse response can be seen in the time series of the gearbox vibration data, the size of the fault can be diagnosed. Al-Dossary et al. [35] also observed two large spikes in their experiments. The first spike is initiated when the roller element enters the defect and the second spike is produced when the roller element exits the defect. From their analysis, it can be postulated that time duration between the two impulses is proportional to the defect size. However, this is not usually possible to quantify because of the presence of background noise, and the location of entry point and exit point cannot be determined accurately. Thus, an advanced signal processing is needed to filter out the original signal from its background noise.

In this section AE signals are sampled at a rate of 2 MHz for maximum accuracy in detecting the entry and exit points. The size

of the artificial line shape defects were 1 mm (D1) and 2 mm (D2) in width and 0.5 mm in depth. For measured AE signals the experiments were conducted at speeds of 600 rpm (S2) and 1100 rpm (S3) and under loads of 0 N (L0) and 100 N (L1) to investigate the effects of speed and load on the AE defect size estimation. The time duration of measured AE waveform is selected as 3 s (6,000,000 data points). The theoretical defect size on the outer race can be calculated based on shaft rotating speed and relative velocities of outer race and roller elements. The objective is to correlate the theoretical and artificial defect size. The schematic of bearing components with an outer race defect is shown in Fig. 18. The relative velocity of roller elements and the outer race is known as cage frequency which can be calculated by Eq. (27) [3]:

$$F_{FTF} = \frac{f_s}{2} \left(1 - \left(\frac{BD}{PD} \right) \cos \beta \right) \quad (27)$$

A typical line defect on the outer race of a bearing can be represented either with its length or its associated angle. This angle can be calculated by measuring the angle between the lines connecting the center of the bearing to the either side of the line fault as follows:

$$\Delta\theta = F_{FTF} \times \Delta t = \frac{f_s}{2} \left(1 - \left(\frac{BD}{PD} \right) \cos \beta \right) \Delta t = \frac{2L}{(PD + BD)} \quad (28)$$

where L is the defect size and Δt is time travel duration between two spikes. f_s is the shaft rotating speed in (rad/s) and β is the contact angle. The above Equation can be simplified into the compact form of:

$$L = \frac{f_s}{4F} \left[\frac{(PD + BD)(PD - BD \times \cos \beta)}{PD} \right] \quad (29)$$

where $F = 1/\Delta t$ is the frequency between two spikes in Hz. Defect size on the inner race and roller elements can be defined by Eqs. (30) and (31) respectively. Appendix A provides the mathematical calculation of defect size for the inner race and the roller elements (see Fig. 19).

$$L = \frac{f_s}{4F} \left[\frac{(PD - BD)(PD + BD \times \cos \beta)}{PD} \right] \quad (30)$$

$$L = \frac{f_s}{4F} (PD - BD \times \cos \beta) \quad (31)$$

The measured AE signals are processed using the proposed method for de-noising along with spectral analysis of the squared Hilbert transform. A window size of 2200 point is selected to measure the time duration and frequency between two spikes of each double impulses. After the AE frequencies (F) of all double spikes are successfully found, the arithmetic mean of all AE frequencies is calculated and reported as the experimentally measured AE frequency (F_{ave}). By substituting the F_{ave} in Eqs. (29)–(31) the artificial fault size on different locations can be measured. Defect size calculations on different locations can be seen in Figs. 20–22. Measured defect sizes obtained from AE signals under different conditions are tabulated in Tables 12–14 for comparison purposes.

It can be concluded that estimated defect size of measured data is not sensitive to the loading condition and rotating speed of the bearing. As it can be seen from Tables 12–14 the relative error does not exceed 10% in any cases. It shall be noted that one major source of the deviation in experimentally found values of defect sizes compared to the actual sizes is due to the unrealistic assumption of no slip condition between rolling element bearing components that is used to derive the theoretical equations.

9. Conclusions and remarks

For sensitivity analysis of AE parameters, DOE method was employed. Plackett–Burman method was chosen as the design table to provide the pattern for scaling the parameters. The results of AE parameter analysis based on DOE demonstrate that, skewness and number of AE counts are the most suitable parameters for detecting incipient faults under different conditions for the outer race. However, if the rotating speed of the shaft is constant, burst duration and RMS are the most powerful statistical parameters to diagnose incipient faults. For defect size growth crest factor was determined as the most sensitive parameter to the defect size under different conditions; however, the influence of rotating speed on crest factor cannot be neglected. Moreover, variation of loading conditions on the bearing has no obvious influence on the AE parameters. It has to be noted that, AE counts is the recommended parameter to monitor defect size growth on the outer race under constant rotating speed.

Feature enhancement of the weak signature from the noisy signal is essential to fault prognostics, in which case features are often very weak and masked by the background noise. This paper presents a new approach of optimizing wavelet functions based on maximizing the KER value, and selecting the optimal band pass filter signal using KER calculation of WPT band-pass signals to detect bearing faults. The proposed method is well suited for detecting the weak signature from a defective bearing signal where defect features are impulse-like. The simulated bearing fault signal which was completely masked by the noise was enhanced and the characteristic frequency was successfully detected using envelope spectrum. Also, experimental results verified the effectiveness of the proposed method by measuring the fault frequency on the outer race, inner race, and roller elements under varying rotating speeds, loadings, and defect sizes. The weak periodic impulse signatures were successfully enhanced and experimental fault frequencies compared with their theoretical values which revealed a maximum error of 3%.

To estimate the defect size, the proposed method was utilized to de-noise the noisy measurement data. Then spectrum of squared Hilbert transform was performed to measure the time travel between double impulses for calculating the defect sizes at different locations. Experimental measured defect sizes were compared with their actual values which shown a maximum error of 10%.

Acknowledgments

Authors thank to Dr. Phani and Mohammad Miraskari for fruitful discussions. This research project was supported by Grants from the Qatar National Research Fund (QNRF), Doha, Qatar.

Appendix A. Calculation of defect size on Inner race and rolling elements

A.1. Defect size calculation for the inner race

See Fig. A.1

$$\begin{aligned} \Delta\theta = (f_s - F_{FTF})\Delta t &= \left[f_s - \frac{f_s}{2} \left(1 - \left(\frac{BD}{PD} \right) \cos \beta \right) \right] \Delta t \\ &= \frac{2L}{(PD - BD)} \end{aligned} \quad (A.1)$$

$$L = \frac{f_s}{4F} \left[\frac{(PD - BD)(PD + BD \times \cos \beta)}{PD} \right] \quad (A.2)$$

A.2. Defect size calculation for the roller element

See Fig. A.2

$$\Delta\theta = F_{FTF} \left(\frac{PD}{BD} \right) \Delta t = \frac{f_s}{2} \left(\frac{PD - BD \times \cos\beta}{PD} \right) \left(\frac{PD}{BD} \right) \Delta t = \frac{2L}{BD} \quad (\text{A.3})$$

$$L = \frac{f_s}{4F} (PD - BD \times \cos\beta) \quad (\text{A.4})$$

References

- [1] McFadden P, Smith J. Model for the vibration produced by a single point defect in a rolling element bearing. *J Sound Vib* 1984;96:69–82.
- [2] Pao YH, Gajewski RR, Ceraoglu AN. Acoustic emission and transient waves in an elastic plate. *J Acoust Soc Am* 1979;65:96.
- [3] Tandon N, Choudhury A. A review of vibration and acoustic measurement methods for the detection of defects in rolling element bearings. *Tribol Int* 1999;32:469–80.
- [4] Mba D, Rao RBKN. Development of acoustic emission technology for condition monitoring and diagnosis of rotating machines; bearings, pumps, gearboxes, engines and rotating structures. 2006.
- [5] Al-Ghamdi AM, Mba D. A comparative experimental study on the use of acoustic emission and vibration analysis for bearing defect identification and estimation of defect size. *Mech Syst Sig Process* 2006;20:1537–71.
- [6] Dyer D, Stewart R. Detection of rolling element bearing damage by statistical vibration analysis, 1977.
- [7] Antoni J, Randall R. The spectral kurtosis: application to the vibratory surveillance and diagnostics of rotating machines. *Mech Syst Sig Process* 2006;20:308–31.
- [8] Sawalhi N, Randall R, Endo H. The enhancement of fault detection and diagnosis in rolling element bearings using minimum entropy deconvolution combined with spectral kurtosis. *Mech Syst Sig Process* 2007;21:2616–33.
- [9] Yiakopoulos C, Antoniadis I. Wavelet based demodulation of vibration signals generated by defects in rolling element bearings. *Shock Vib* 2002;9:293–306.
- [10] Qiu H, Lee J, Lin J, Yu G. Wavelet filter-based weak signature detection method and its application on rolling element bearing prognostics. *J Sound Vib* 2006;289:1066–90.
- [11] Zarei J, Poshtan J. Bearing fault detection using wavelet packet transform of induction motor stator current. *Tribol Int* 2007;40:763–9.
- [12] Lei Y, Lin J, He Z, Zi Y. Application of an improved kurtogram method for fault diagnosis of rolling element bearings. *Mech Syst Sig Process* 2011.
- [13] Martin H, Honarvar F. Application of statistical moments to bearing failure detection. *Appl Acoust* 1995;44:67–77.
- [14] Gustafsson OG, Tallian T. Detection of damage in assembled rolling element bearings. *ASLE TRANSACTIONS* 1962;5:197–209.
- [15] Montgomery DC. Design and analysis of experiments. John Wiley & Sons Inc; 2008.
- [16] Li Y, Billington S, Zhang C, Kurfess T, Danyluk S, Liang S. Adaptive prognostics for rolling element bearing condition. *Mechanical Systems and Signal Processing* 1999;13:103–13.
- [17] Wu Y, Du R. Feature extraction and assessment using wavelet packets for monitoring of machining processes. *Mech Syst Sig Process* 1996;10:29–53.
- [18] Wu JD, Liu CH. An expert system for fault diagnosis in internal combustion engines using wavelet packet transform and neural network. *Expert Syst Appl* 2009;36:4278–86.
- [19] Zhang J, Walter GG, Miao Y, Lee WNW. Wavelet neural networks for function learning. *Sig Process, IEEE Trans* 1995;43:1485–97.
- [20] Shannon C, Weaver W. The mathematical theory of communication. Univ. of Illinois Press; 1949.
- [21] Ihara S. Information theory for continuous systems, vol. 2. World Scientific Pub Co Inc; 1993.
- [22] Dwyer R. Detection of non-Gaussian signals by frequency domain kurtosis estimation. 1983. p. 607–10.
- [23] Antoni J. The spectral kurtosis: a useful tool for characterising non-stationary signals. *Mech Syst Sig Process* 2006;20:282–307.
- [24] Antoni J. Fast computation of the kurtogram for the detection of transient faults. *Mech Syst Sig Process* 2007;21:108–24.
- [25] Cizek V. Discrete hilbert transform. *Audio Electroacoust, IEEE Trans* 1970;18:340–3.
- [26] Yang WX, Ren XM. Detecting impulses in mechanical signals by wavelets. *EURASIP J Appl Sig Process* 2004;2004:1156–62.
- [27] Singh BN, Tiwari AK. Optimal selection of wavelet basis function applied to ECG signal denoising. *Digital Sig Process* 2006;16:275–87.
- [28] Cover TM, Thomas JA, Wiley J. Elements of information theory, vol. 6. Wiley Online Library; 1991.
- [29] Abry P. Ondelettes et turbulences: multirésolutions, algorithmes de décomposition, invariance d'échelle et signaux de pression. Diderot multimédia; 1997.
- [30] Donoho DL. De-noising by soft-thresholding. *Inform Theory, IEEE Trans* 1995;41:613–27.
- [31] Ericsson S, Grip N, Johansson E, Persson LE, Sjöberg R, Strömberg JO. Towards automatic detection of local bearing defects in rotating machines. *Mech Syst Sig Process* 2005;19:509–35.
- [32] Teolis A. Computational signal processing with wavelets. Birkhäuser; 1998.
- [33] Prashad H. The effect of cage and roller slip on the measured defect frequency response of rolling-element bearings. *ASLE TRANSACTIONS* 1987;30:360–7.
- [34] Epps I, McCallion H. An investigation into the characteristics of vibration excited by discrete faults in rolling element bearings. 1994.
- [35] Al-Dossary S, Hamzah R, Mba D. Observations of changes in acoustic emission waveform for varying seeded defect sizes in a rolling element bearing. *Appl Acoust* 2009;70:58–81.